1 **Extracellular electron transfer mediated by a cytocompatible redox polymer**

2 **lengthens the circadian period of mammalian cells**

3 Masahito Ishikawa[1,4]*, Kazuki Kawai[1], Masahiro Kaneko[2], Kenya Tanaka[3], Shuji

4 Nakanishi[3, 4], and Katsutoshi Hori[1]*

5

6 [1]Department of Biomolecular Engineering, Graduate School of Engineering, Nagoya

7 University, Furo-cho, Chikusa-ku, Nagoya 464-8603, Japan

8 [2]Department of Materials Engineering, School of Engineering, The University of Tokyo,

9 7-3-1 Hongo, Bunkyo-ku, Tokyo 113-8656, Japan

10 [3]Graduate School of Engineering Science, Osaka University, 1-3 Machikaneyama,

11 Toyonaka, Osaka 560-8631, Japan

12 [4]Research Center for Solar Energy Chemistry, Osaka University, 1-3 Machikaneyama,

13 Toyonaka, Osaka 560-8631, Japan

14

15 *Corresponding authors

16 E-mail address

17 ishikawa.masahito@chembio.nagoya-u.ac.jp (M. I.)

18 khori@chembio.nagoya-u.ac.jp (K. H.)

19

22

Abstract

The crosstalk among the circadian clock, cellular metabolism, and cellular redox state has attracted much attention. To elucidate this crosstalk, chemical compounds have been used to perturb cellular metabolism and the redox state. However, extracellular electron transfer (EET) with an electron mediator has not been used to study the mammalian circadian clock due to potential cytotoxic effects of the mediator. Here, we describe the use of EET mediated by pMFc, a cytocompatible redox polymer, on human U2OS cells. EET mediated by oxidized pMFc (ox-pMFc) extracted intracellular electrons, resulting in a longer circadian period. Analyses of the metabolome and intracellular redox species suggest that ox-pMFc receives an electron from glutathione, thereby inducing pentose phosphate pathway activation. We anticipate that redox perturbation via EET will provide new insights into the crosstalk among the circadian clock, metabolism, and redox state, which may lead to the development of new treatments for circadian clock disorders.

Introduction

The circadian clock is a biological system that generates an approximately 24-hour cell-autonomous rhythm for the purpose of anticipating periodic changes in the environment and enabling organisms to adapt to such predictable changes[1]. The mammalian circadian clock is driven by transcriptional–translational feedback loops composed of clock genes. In the core feedback loop, the transcription factors BMAL1 and CLOCK, or the closely related homolog NPAS2, activate expression of the genes *Period* (*Per1* and *Per2*) and *Cryptochrome* (*Cry1* and *Cry2*). After translation and nuclear localization, PER and CRY proteins inhibit the function of either the BMAL1/CLOCK or BMAL1/NPAS2 heterodimer, closing the negative feedback loop. Because BMAL1/CLOCK and BMAL1/NPAS2 also regulate the transcription of other genes, various physiological and cellular processes, including metabolism, exhibit circadian rhythms. Studies have implied that metabolic rhythm is not only a simple output of circadian regulation, but also provides important input to the circadian clock, which is essential for maintaining the robustness of the circadian clock[1b, 2]. Therefore, in order to achieve a comprehensive understanding of the circadian clock system, it is very important to elucidate the crosstalk between metabolism and the circadian clock.

Metabolic perturbations that modulate the circadian clock are useful for a good understanding of the crosstalk between metabolism and the circadian clock. Redox state perturbation is also effective because metabolism is a network of biochemical reactions accompanied by electron transfers and the intracellular redox state is closely related to cellular metabolism. Redox/metabolic perturbations using redox-active molecules or inhibitors against metabolic enzymes have been employed; such perturbations have provided new insights into how the redox state and metabolism are related to the circadian clock system[3]. Therefore, the use of chemical compounds capable of inducing redox state and metabolic alternations has been identified as a promising approach for studying the circadian clock. The discovery and development of such

65 chemical compounds will contribute to a comprehensive understanding of the circadian

66 clock system, and may lead to new treatments for diseases caused by circadian clock

67 disorders.

68   The construction of an extracellular electron transfer (EET) pathway, in which the

69 intracellular electrons are exchanged with an extracellular electron donor/acceptor

70 across the cell membrane, is an effective approach for altering intracellular redox

71 balance and cellular metabolism[4]. The EET pathway can be constructed using a

72 membrane-permeable redox-active compound, namely, an electron mediator[5].

73 Modifications of intracellular redox balance via EET have been demonstrated in many

74 microbial species[6]. Nevertheless, the use of EET as a redox/metabolic perturbation has

75 been limited in mammalian studies possibly due to the cytotoxic effects of electron

76 mediators.   To   date,   we   have   demonstrated   that   2-methacryloyloxyethyl

77 phosphorylcholine (MPC)-based redox polymers are cytocompatible electron mediators

78 that can alter the intracellular redox states and metabolism of several microbial

79 species[7]. For example, the metabolism of *Saccharomyces cerevisiae* was altered by

80 extracting intracellular electrons with the oxidized form of pMFc (ox-pMFc, where

81 pMFc is poly MPC-*co*-vinyl ferrocene, E_M = +0.5 V vs. SHE)[7c]. Hence, we assumed

82 that EET mediated by ox-pMFc can also alter the intracellular redox state and

83 metabolism of mammalian cells, thereby altering the mammalian circadian clock

84 (Figure 1).

85   Here, we report for the first time, evidence that EET, facilitated by a

86 cytocompatible electron mediator based on MPC, can be used to study the mammalian

87 circadian clock.

88

89
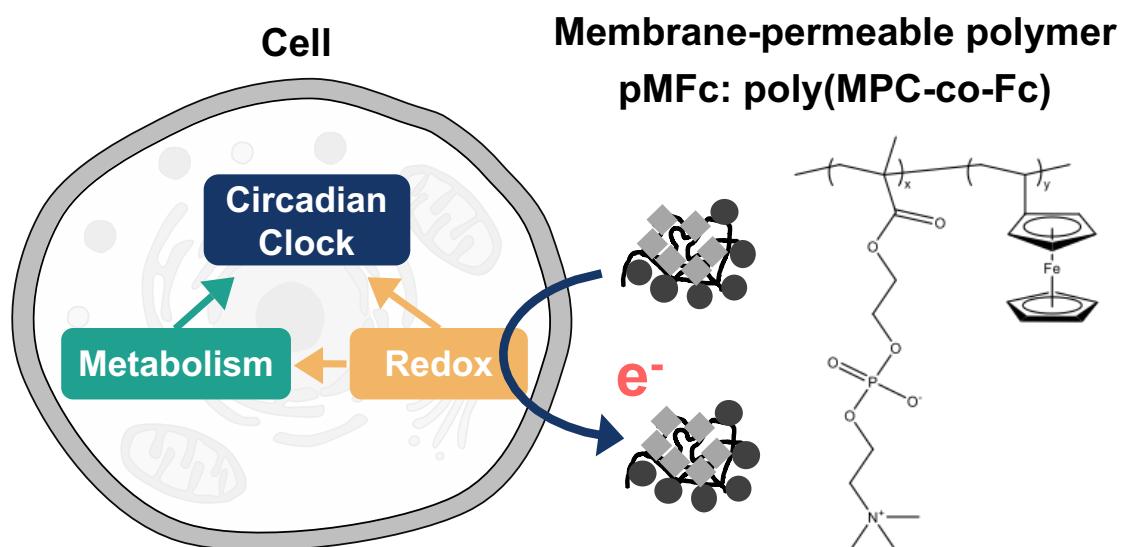
90   ***Figure 1.*** Schematic of the concept in this study. The oxidized form of pMFc

91   (ox-pMFc) crosses the plasma membrane of a living U2OS cell and accepts an electron

92   from intracellular redox species, resulting in the alternation of the cellular redox state.

93   This redox perturbation affects the circadian clock either directly, indirectly, or both

94   ways through the metabolic alternation induced by the redox state alternation.

95

96   **Results and Discussion**

97   **EET via pMFc in U2OS cells**

98   To verify the feasibility of our approach, we began by determining if ox-pMFc can

99   accept an electron from human osteosarcoma U2OS cells, which is a well-characterized

100   cell line for circadian clock research. The UV/Vis absorption spectrum of ox-pMFc in

101   the medium displays a characteristic peak at 620 nm, in contrast to the reduced form of

102   pMFc (red-pMFc) in the medium (Figure S1a). Hence, the abundance of ox-pMFc in

103   the medium can be determined by the absorbance of the medium at 620 nm (A_{620}). We

104   exchanged the cultivation medium of confluent U2OS cells with the medium containing

105   1 mM ox-pMFc, incubated at 37°C supplemented with CO_2, and measured the A_{620} of

106 the medium at the indicated time points (Figure S1b). The abundance of ox-pMFc

107 gradually decreased, indicating the reduction of ox-pMFc by accepting an electron from

108 reductive species. Although the reduction of ox-pMFc was also observed in the absence

109 of U2OS cells, the complete reduction of ox-pMFc was faster in the presence of U2OS

110 cells than in their absence; complete reduction required 24 h in the presence of U2OS

111 cells and 72 h in their absence. This result means that ox-pMFc molecules accept

112 electrons not only from cells but also from redox species in the medium. Commercial

113 media generally contain numerous reductive compounds as antioxidants, such as

114 vitamins. We deduced that these compounds donate electrons to ox-pMFc molecules.

115 The abundance of the ox-pMFc was 84.5% in the presence compared with 89.2% the

116 absence of U2OS cells after the first hour of incubation. Therefore, 4.7% ox-pMFc

117 (47.7 μM) accepted electrons from the U2OS cells during the first 1 h.

118   Next, we tested if the ox-pMFc can accept an electron from representative

119 intracellular redox species *in vitro*, namely the reduced form of glutathione (GSH),

120 NADH, and NADPH (Figure S1c). As controls, we used the oxidized form of

121 glutathione (GSSG), NAD^+, and $NADP^+$. Immediately after 1 mM of each compound

122 was mixed with a 1 mM ox-pMFc solution, A_{620} of the mixture was measured with a

123 spectrophotometer over time. We observed a decrease in A_{620} when ox-pMFc was

124 mixed with the reduced forms of these redox species, whereas A_{620} did not change when

125 ox-pMFc was mixed with its oxidized forms, indicating that the ox-pMFc can accept

126 electrons from the reduced form of these compounds in living cells.

127

128 **Effect of ox-pMFc-mediated EET on the circadian clock in U2OS cells**

129   To investigate the effect of EET mediated by ox-pMFc on the mammalian circadian

130 clock, we performed a cell-based luminescence assay using U2OS cell lines harboring a

131 *Bmal1–dLuc* reporter[8]. The bioluminescence was monitored with 0.25–1.5 mM

132 ox-pMFc (Figure S2). Although ox-pMFc caused period lengthening in a

dose-dependent manner, it became difficult to extract peaks or troughs from the
bioluminescence rhythm at high concentrations (1.25–1.50 mM). Because the reporter
activity of *Bmal1–dLuc* is dependent on cell viability, a high concentration of ox-pMFc
may be cytotoxic towards U2OS cells. Thus, we determined the effect of less than 1
mM ox-pMFc on the circadian clock of U2OS cells. The detrended bioluminescence
rhythm clearly indicated that the ox-pMFc lengthened the period of the circadian clock
in U2OS cells (Figure 2a). Since the abundance of ox-pMFc in the medium decreased
gradually as shown in Fig. S1b, the effect of ox-pMFc-mediated EET should change
with duration. The period changes relative to the control were analyzed as a period of
each day, namely, a period between one trough and the next, or one peak and the next
peak (Figure 2b).

For the first two days after ox-pMFc treatment, the periods lengthened in a
dose-dependent manner. Thereafter, the periods of cells treated with lower
concentrations of ox-pMFc (0.25 and 0.5 mM) were restored to their original length,
whereas those at higher concentrations (0.75 mM and 1 mM) maintained an
approximately 1 h extension. When U2OS cells were treated with red-pMFc, which
cannot accept electrons from cells, the circadian period was hardly altered (Figure 2cd).
These remarkably different results obtained with different redox forms of pMFc suggest
that EET induced the observed period lengthening.

As shown in Fig. S1b, ox-pMFc accepts an electron not only from intracellular
redox species in U2OS cells but also from redox-active components in the medium. We
assumed that oxidation of the medium by ox-pMFc affects the circadian clock of U2OS
cells. To confirm this, we determined if the medium oxidized by ox-pMFc lengthens the
circadian period. The medium for measuring bioluminescence rhythm was mixed with
each concentration of ox-pMFc in the absence of U2OS cells, and incubated at 37°C
supplemented with 5% CO_2 for 3 d. The complete reduction of ox-pMFc was verified
by measuring the A_{620} of the medium. The bioluminescence rhythm of U2OS cells was

monitored after exchanging the cultivation medium with these oxidized media. The graph in Fig. 2e seems to show little difference between the control and samples treated with the oxidized media. When the change in period relative to the control was measured, we observed an approximately 1 h longer period lengthening only in U2OS cells treated with medium oxidized by 1 mM ox-pMFc. Other oxidized media did not alter the U2OS circadian period, indicating that the oxidation of media components affects the circadian period of U2OS to a lesser extent than EET via ox-pMFc.
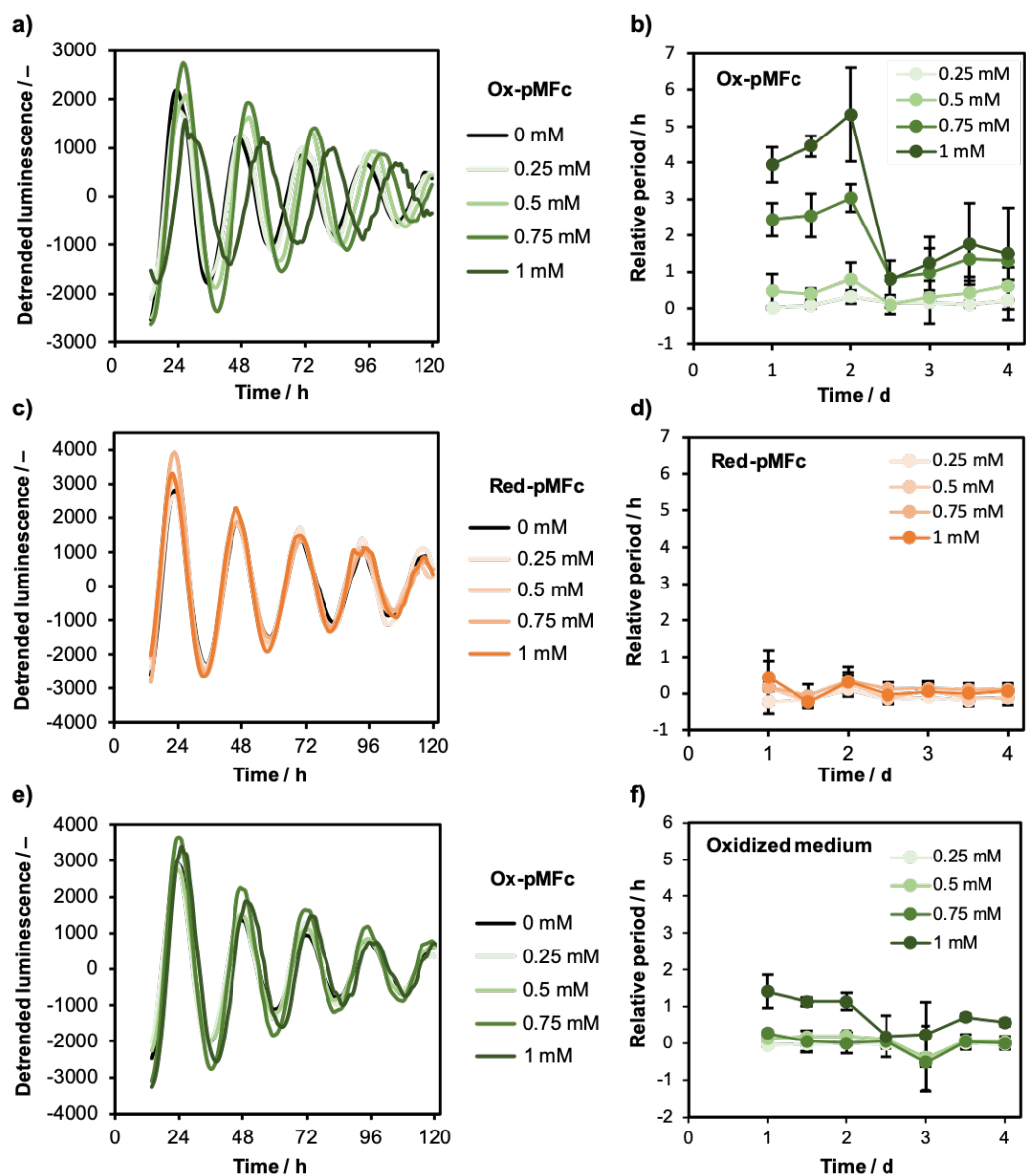
168 *Figure 2*. Effect of pMFc-mediated EET on the circadian clock in U2OS cells.

169 Representative curves of the detrended bioluminescence rhythms of

170 U2OS::*Baml1–dLuc* cells in the presence of a) ox-pMFc or c) red-pMFc, or e) in the

171 medium oxidized by ox-pMFc. b, d, f) Changes in the circadian period length relative to

172 10 mM HEPES buffer control. The period length was calculated as the time between

173 either one trough and the next, or between one peak and the next. Each concentration of

174 pMFc corresponds to that of the vinyl ferrocene unit. Data are expressed as means ± SD

175 ($n = 3$).

176

177 **Metabolic and redox alternations induced by ox-pMFc-mediated EET**

178 To investigate which metabolic alternations were induced by the

179 ox-pMFc-mediated EET, metabolites were extracted from U2OS cells after 24 h

180 treatment with either 1 mM ox- or red-pMFcs and were analyzed comprehensively. We

181 assumed that the metabolic profiles after the 24 h treatment should be altered because

182 the abundance of ox-pMFc remains at about 12% (Figure S1b) and the period was

183 lengthened by approximately 4 h (Figure 2b). Following our metabolomic analysis, 116

184 peaks (52 cations and 64 anions) were detected by the anion and cation modes of

185 CE-TOFMS and CE-QqQMS. The results of principal component analysis (PCA) and

186 hierarchical cluster analysis (HCA) are shown in Fig. S3. The PCA revealed that PC1

187 (horizontal axis) distinctly separated the samples treated with 1 mM ox-pMFc from the

188 samples treated with 1 mM red-pMFc and untreated samples (control). PC2 (vertical

189 axis) clarified the differences between the same samples, suggesting that there is an

190 outlier among the red-pMFc-treated samples. HCA revealed that the metabolic patterns

191 of 1 mM red-pMFc-treated cells and untreated cells were similar, whereas those of 1

192 mM ox-pMFc-treated cells was distinct, implying that the metabolic alternation was

193 induced by ox-pMFc-mediated EET. The metabolic pathways and metabolites

194 associated with glycolysis/gluconeogenesis, the pentose phosphate pathway (PPP), and

9

the tricarboxylic acid (TCA) cycle are illustrated in Fig. 3. The concentrations of some metabolites associated with PPP increased significantly in cells treated with 1 mM ox-pMFc, whereas those with glycolysis and TCA cycle decreased significantly. The results of metabolomic analysis indicate the activation of PPP by EET via ox-pMFc.
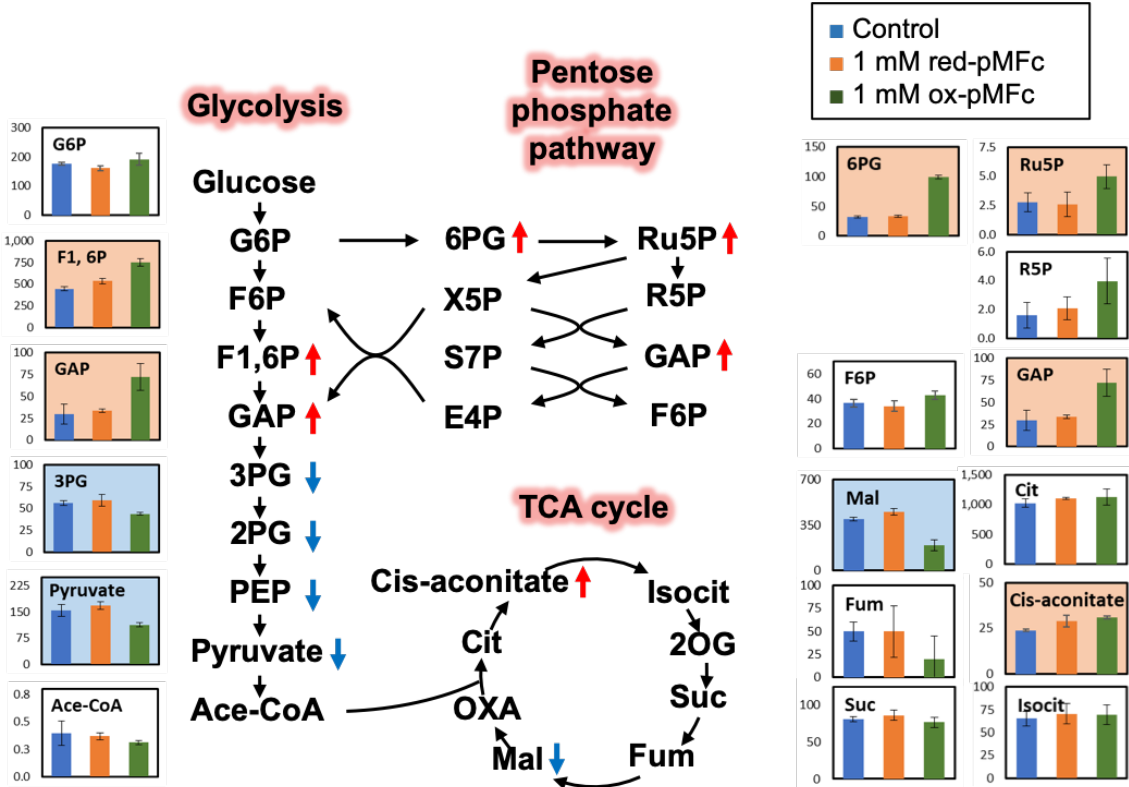
Figure 3. Metabolic alternation of U2OS cells induced by ox-pMFc-mediated EET for 24 h. The metabolic pathways and metabolites associated with glycolysis/gluconeogenesis, the pentose phosphate pathway, and the tricarboxylic acid (TCA) cycle are shown. The vertical axis in the graphs indicates the absolute concentration of metabolites (mol/10^6 cells). Significant differences were examined by Welch's *t*-test (control versus the ox-pMFc-treated cells). The concentration of pMFc corresponds to that of vinyl ferrocene unit. The significantly altered metabolites ($p < 0.05$) are highlighted by red (increase) or blue (decrease) color. Data are shown as

209   means ± SD ($n = 3$).

210

211   PPP is a pathway to provide NADPH, which serves as reducing power for

212   regenerating GSH from GSSG. We assumed that the ratios of NADPH:NADP$^+$ and

213   GSH:GSSG should be altered by EET via the ox-pMFc. Figure 4 shows time courses of

214   the GSH:GSSG and NADPH:NADP$^+$ ratios in U2OS cells treated with either 1 mM ox-

215   or red-pMFc and in untreated cells (control). For the first 3 h, the GSH:GSSG ratio in

216   ox-pMFc-treated cells was significantly lower than those in red-pMFc-treated cells and

217   control cells. The GSH:GSSG ratio in ox-pMFc-treated cells subsequently became the

218   same level as that in the other cells at 6 h before finally becoming more reductive than

219   that in the other cells (Figure 4). On the other hand, the NADPH:NADP$^+$ ratio in

220   ox-pMFc-treated cells was always higher than that of the other samples.

221

222
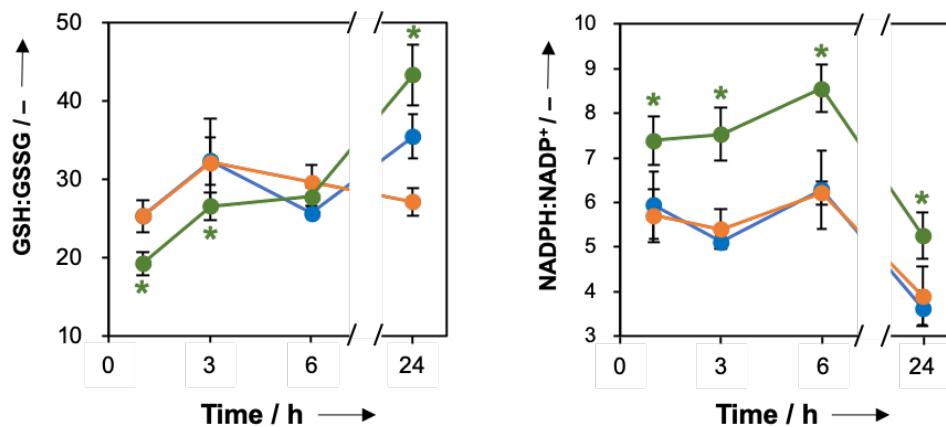
223   *Figure 4.* Time course alternations of the ratios of a) GSH:GSSG and b)

224   NADPH:NADP$^+$ in U2OS cells. Data are expressed as mean ± SD ($n = 3$). Asterisks

225   indicate the significant difference (Waltch's t-test, control verses the pMFc-treated cells,

226    $p < 0.05$).

227

11

228   The alternations of GSH:GSSG and NADPH:NADP$^+$ ratios suggested that

229   ox-pMFc accepted an electron mainly from intracellular GSH. As GSH is more

230   abundant in the cytosol than other redox species such as NADH and NADPH[9], it is the

231   most likely redox molecule that pMFc molecules passing through the membrane will

232   encounter first. U2OS cells whose GSH:GSSG ratio became oxidative are thought to

233   activate their PPP in order to maintain the redox balance, resulting in a higher ratio of

234   NADPH:NADP$^+$. As the abundance of ox-pMFc gradually decreased and stayed low for

235   24 h (Figure S1b), little reduction in GSH should have occurred at 24 h. According to

236   the result of metabolomic analysis (Figure 3), PPP remained activated in

237   ox-pMFc-treated cells after 24 h. Hence, the GSH:GSSG ratio in ox-pMFc-treated

238   U2OS cells were thought to recover to the same level as the other samples at 6 h and

239   become more reductive than other samples at 24 h.

240   The metabolic profile of the 1 mM ox-pMFc-treated U2OS cells reflected the

241   homeostasis for an intracellular redox balance. Homeostatic changes to metabolism

242   were thought to induce the period-lengthening of circadian rhythm in U2OS cells.

243   Based on *in vitro* experiments using the purified transcriptional factors, Rutter et al.

244   reported that NADPH enhanced DNA binding of CLOCK:BMAL1 and

245   NPAS2:BMAL1 heterodimers[10]. Hence, the increase in NADPH:NADP$^+$ ratio by PPP

246   activation might enhance the DNA-binding activity of CLOCK:BMAL1 and

247   NPAS2:BMAL1 heterodimers in U2OS cells. Rey et al. reported that PPP inhibition

248   induces an oxidative NADPH:NADP$^+$ ratio and lengthens the circadian period in U2OS

249   cells. They thereby proposed that PPP is an important regulator of the circadian

250   rhythm[3a]. Conversely, our results show that the circadian period was lengthened in

251   U2OS cells whose NADPH:NADP$^+$ ratio was increased by PPP activation. Although

252   our results also indicate that PPP is important for regulating the circadian clock, the

253   intracellular redox state and metabolism of U2OS cells that showed period-lengthening

254   differ from those reported by Rey et al. Therefore, our study suggests the existence of

255   an undefined mechanism underlying the regulation of the circadian clock by the cellular

256   redox state and metabolism. Elucidation of this mechanism will require further study.

257   In summary, we have demonstrated that ox-pMFc-mediated EET induced metabolic

258   alternations, resulting in lengthening of the circadian period in U2OS cells. Our results

259   suggest that MPC-based redox polymers such as pMFc are applicable to studies of the

260   mammalian circadian clock. Because MPC-based polymers are flexible in their design,

261   electron mediators with either different redox potentials or reactivities can be

262   synthesized[7c, 7d, 11]. We anticipate that the use of various MPC-based redox polymers

263   will provide new insights to improve understanding of the crosstalk among the circadian

264   clock, cellular metabolism, and cellular redox state, which may subsequently impact the

265   development of new treatments for diseases caused by circadian clock disorders.

266

267   **Experimental Section**

268   *Chemicals*

269   NAD^+, NADH, $NADP^+$, and NADPH were purchased from Oriental Yeast Co., ltd

270   (Tokyo, Japan). GSH and GSSG were purchased from Nacalai Tesque (Kyoto, Japan).

271   MPC was purchased from NOF Co., Ltd., (Tokyo, Japan). VFc and

272   α,α′-azobisisobutyronitrile (AIBN) were purchased from Wako Pure Chemicals Co., Ltd.

273   (Osaka, Japan) and Kanto Chemical Co., Inc. (Tokyo, Japan), respectively. AIBN was

274   recrystallized in methanol before use. pMFc was synthesized using 3.54 g MPC and

275   1.70 g VFc by conventional free radical polymerization with 164 mg AIBN as an

276   initiator in 20 mL ethanol. Polymerization was conducted in a test tube at 65°C for 48 h

277   under an argon gas atmosphere. After the polymerization reaction, the polymer solution

278   was precipitated with a mixed solvent composed of diethyl ether/chloroform (90:10,

279   v/v). The polymer precipitate was filtered and dried in a vacuum overnight. The

280   polymer was subsequently dissolved in distilled water and dialysis was performed for 4

281   d. The polymers were freeze-dried, and the resulting yellow powder was obtained as

282 reduced pMFc polymer. Molecular weight was measured by gel permeation

283 chromatography with poly(ethylene glycol) as a standard. The composition was

284 determined by UV/Vis spectroscopy. To prepare ox-pMFc, red-pMFc was dissolved in

285 20 mM HEPES buffer at final concentration of 4 mM (corresponds to the concentration

286 of the VFc unit in pMFc) and electrochemically oxidized at +0.6 V for 20 h, with

287 stirring. Oxidization of red-pMFc was confirmed by measuring A_{620}.

288

289 *Mammalian cell culture*

290 Human osteosarcoma U2OS cell lines harboring a *Bmal1–dLuc* reporter[8a] was

291 kindly provided by T. Nishiwaki-Ohkawa and T. Yoshimura from Nagoya University.

292 Cells were maintained at 37°C under 5% CO_2 and 95% air in DMEM (1199560,

293 Thermo Fisher Scientific Inc, Waltham, MA, USA) supplemented with 100 μg/mL

294 penicillin, 100 μg/mL streptomycin, and 10% fetal bovine serum (FBS).

295 To determine ox-pMFc reactivity towards cells, U2OS reporter cells were cultivated

296 to confluence on a 35-mm dish with a 9 cm^2 surface area (MS-11350, Sumitomo

297 Bakelite Co., Ltd., Tokyo, Japan). The medium was replaced with 2.6 mL of medium

298 for recoding bioluminescence rhythms, which is composed of DMEM (D2902,

299 Sigma-Aldrich, St. Louis, MO, USA) supplemented with 10% FBS, 3.5 g/L D-glucose,

300 0.35 g/mL sodium hydrogen carbonate, 100 μg/mL penicillin, 100 μg/mL streptomycin,

301 0.1 mM luciferin, 100 nM dexamethasone, 10 mM HEPES (pH7.0), and 1 mM

302 ox-pMFc (corresponds to the concentration of the VFc unit in pMFc). The abundance of

303 ox-pMFc was estimated by measuring the A_{620} of the medium.

304 For real-time monitoring of the cellular bioluminescence rhythms, U2OS reporter

305 cells were cultivated to confluence on a 60-mm dish with 21 cm^2 surface area

306 (CELLSTAR, Greiner Bio-One International GmbH, Kremsmünster, Germany). The

307 medium was replaced with 6 mL of the medium used for recoding the bioluminescence

308 rhythms. When required, the medium contained either ox- or red-pMFc at the different

309   concentrations (0.25–1.5 mM). Bioluminescence signals of the cultured cells were

310   recorded at intervals of 1 h at 37°C in air with a Gene Light 55 GL-100A luminometer

311   (Microtec Co., Ltd., Chiba, Japan).

312

313   *Calculation of circadian period*

314   Raw data obtained by measuring bioluminescence rhythms were detrended by

315   subtracting their 24 h moving averages. To calculate the period length for each day, the

316   detrended 24 h data was fitted to a cosine curve with the following equation

317
$$y = (mx + c) + \alpha e^{-kx} \cos\left(\frac{2\pi x - r}{p}\right)$$
318

319   where m is the gradient of the baseline, c is the y offset, k describes the damping rate, α

320   is the amplitude, r is the phase, and p is the period. Curve-fitting was performed by the

321   least squares method using the Solver function of Microsoft Excel.

322

323   In vitro *reaction of ox-pMFc with NADH, NADPH, and GSH*

324   One hundred milliliters of 1 mM ox-pMFc (corresponds to the concentration of the

325   VFc unit in pMFc) in 10 mM HEPES buffer was placed into a microcuvette and then set

326   on a spectrometer（UV1850, Simadzu Corporation, Kyoto, Japan）equipped with a

327   microcuvette holder (Shimadzu). Immediately after mixing with 1 mM NADH, NAD^+,

328   NADPH, NADP, GSH, or GSSG, the change in A_{620} in the ox-pMFc solution with time

329   was measured at 1 s intervals.

330

331   *Measurement of intracellular NADPH:$NADP^+$ and GSH:GSSG ratios*

332   Intracellular NADPH:$NADP^+$ and GSH:GSSG ratios were measured using an

333    $NADP^+$/NADPH-Glo Assay kit (Promega) and a GSH/GSSG-Glo Assay kit (Promega),

334   respectively. U2OS cells were prepared and treated with either red- or ox-pMFc using

335   the same procedure for monitoring cellular bioluminescence rhythm. Luminescence was

336 measured with an ARVO X3 (PerkinElmer).

337

338 *Metabolite extraction*

339 U2OS cells were prepared and treated with either ox- or red-pMFc using the same

340 procedure for monitoring the bioluminescence rhythm. As a control, 10 mM HEPES

341 was added to the medium instead of pMFc. After 24 h incubation at 37°C under 5%

342 CO_2, the culture medium was aspirated from a dish. Cells were washed twice with 5%

343 mannitol and treated with 400 μL methanol. The cell extract was treated with 275 μL

344 pure water containing internal standards (H3304-1002, Human Metabolome

345 Technologies (HMT), Tsuruoka, Yamagata, Japan) and left to rest for another 30 s. Cell

346 debris was removed by centrifugation at 200 *g* at 4°C for 5 min and 350 μL of the

347 supernatant was filtered by centrifugation through a Millipore 5-kDa cutoff filter

348 (UltrafreeMC-PLHCC, HMT). Filtrate was concentrated by centrifugation and

349 re-suspended in 50 μL deionized water for metabolomic analysis at HMT.

350

351 *Metabolome analysis*

352 Metabolomic analysis was performed using the *C-SCOPE* package of HMT.

353 Capillary electrophoresis time-of-flight mass spectrometry (CE-TOFMS) was used for

354 cation analysis and CE-tandem mass spectrometry (CE-MS/MS) for anion analysis as

355 described previously[12]. Briefly, CE-TOFMS and CE-MS/MS analysis were carried out

356 using an Agilent CE capillary electrophoresis system equipped with an Agilent 6210

357 time-of-flight mass spectrometer (Agilent Technologies, Waldbronn, Germany) and

358 Agilent 6460 Triple Quadrupole LC/MS, respectively. The systems were controlled by

359 Agilent G2201AA ChemStation software version B.03.01 for CE (Agilent

360 Technologies) and connected by a fused silica capillary (50/μm *i.d.* × 80 cm total length)

361 with a commercial electrophoresis buffer (H3301-1001 and I3302-1023 for cation and

362 anion analyses, respectively, HMT) as the electrolyte. The time-of-flight mass

363 spectrometer was scanned from *m/z* 50 to 1,000[12b] and the triple quadrupole mass

364 spectrometer was used to detect compounds in dynamic MRM mode. Peaks were

365 extracted using MasterHands, automatic integration software (Keio University,

366 Tsuruoka, Yamagata, Japan)[13] and MassHunter Quantitative Analysis B.04.00 (Agilent

367 Technologies) in order to obtain peak information, including *m/z*, peak area, and

368 migration time (MT). Signal peaks were annotated according to the HMT metabolite

369 database based on their *m/z* values with the MTs. The peak area of each metabolite was

370 normalized with respect to the area of the internal standard and metabolite concentration

371 was determined by standard curves with three-point calibrations using each standard

372 compound. Hierarchical cluster analysis (HCA) and principal component analysis

373 (PCA) were performed by HMT's proprietary software, PeakStat and SampleStat,

374 respectively. Any metabolites detected were plotted on metabolic pathway maps using

375 VANTED software[14].

376

386

387 **References**

388 [1]   a) J. C. Dunlap, *Cell* **1999**, *96*, 271-290; b) J. Bass, J. S. Takahashi, *Science*

389   **2010**, *330*, 1349-1354.

390 [2] H. Reinke, G. Asher, *Nat Rev Mol Cell Biol* **2019**, *20*, 227-241.

391 [3] a) G. Rey, U. K. Valekunja, K. A. Feeney, L. Wulund, N. B. Milev, A.

392   Stangherlin, L. Ansel-Bollepalli, V. Velagapudi, J. S. O'Neill, A. B. Reddy, *Cell*

393   *Metab.* **2016**, *24*, 462-473; b) T. Tamaru, M. Hattori, Y. Ninomiya, G.

394   Kawamura, G. Vares, K. Honda, D. P. Mishra, B. Wang, I. Benjamin, P.

395   Sassone-Corsi, T. Ozawa, K. Takamatsu, *PLoS One* **2013**, *8*, e82006; c) Y.

396   Nakahata, S. Sahar, G. Astarita, M. Kaluzova, P. Sassone-Corsi, *Science* **2009**,

397   *324*, 654-657; d) K. A. Feeney, L. L. Hansen, M. Putker, C. Olivares-Yanez, J.

398   Day, L. J. Eades, L. F. Larrondo, N. P. Hoyle, J. S. O'Neill, G. van Ooijen,

399   *Nature* **2016**, *532*, 375-379; e) M. Putker, P. Crosby, K. A. Feeney, N. P. Hoyle,

400   A. S. H. Costa, E. Gaude, C. Frezza, J. S. O'Neill, *Antioxidants & redox*

401   *signaling* **2018**, *28*, 507-520.

402 [4] a) C. I. Torres, A. K. Marcus, H. S. Lee, P. Parameswaran, R. Krajmalnik-Brown,

403   B. E. Rittmann, *FEMS Microbiol Rev* **2010**, *34*, 3-17; b) M. E. Hernandez, D. K.

404   Newman, *Cell. Mol. Life Sci.* **2001**, *58*, 1562-1571; c) F. Kracke, B. Lai, S. Yu, J.

405   O. Kromer, *Metabolic engineering* **2018**, *45*, 109-120.

406 [5] a) K. Watanabe, M. Manefield, M. Lee, A. Kouzuma, *Curr. Opin. Biotechnol.*

407   **2009**, *20*, 633-641; b) B. Huang, S. Gao, Z. Xu, H. He, X. Pan, *Curr. Microbiol.*

408   **2018**, *75*, 99-106.

409 [6] a) K. Sasaki, D. Sasaki, K. Kamiya, S. Nakanishi, A. Kondo, S. Kato, *Curr.*

410   *Opin. Biotechnol.* **2018**, *50*, 182-188; b) S. Kato, *Microbes Environ* **2015**, *30*,

411   133-139; c) B. E. Logan, K. Rabaey, *Science* **2012**, *337*, 686-690.

412 [7] a) K. Nishio, Y. Kimoto, J. Song, T. Konno, K. Ishihara, S. Kato, K. Hashimoto,

413   S. Nakanishi, *Environmental Science & Technology Letters* **2013**, *1*, 40-43; b) Y.

414   Lu, K. Nishio, S. Matsuda, Y. Toshima, H. Ito, T. Konno, K. Ishihara, S. Kato, K.

415   Hashimoto, S. Nakanishi, *Angew. Chem. Int. Ed. Engl.* **2014**, *53*, 2208-2211; c)

416   M. Kaneko, M. Ishikawa, K. Hashimoto, S. Nakanishi, *Bioelectrochemistry*

417   **2017**, *114*, 8-12; d) M. Kaneko, M. Ishikawa, J. Song, S. Kato, K. Hashimoto, S.

418   Nakanishi, *Electrochemistry Communications* **2017**, *75*, 17-20.

419   [8]   a) T. Oshima, I. Yamanaka, A. Kumar, J. Yamaguchi, T. Nishiwaki-Ohkawa, K.

420   Muto, R. Kawamura, T. Hirota, K. Yagita, S. Irle, S. A. Kay, T. Yoshimura, K.

421   Itami, *Angew. Chem. Int. Ed. Engl.* **2015**, *54*, 7193-7197; b) M. Izumo, T. R.

422   Sato, M. Straume, C. H. Johnson, *PLoS Comput Biol* **2006**, *2*, e136.

423   [9]   H. J. Forman, H. Zhang, A. Rinna, *Mol. Aspects Med.* **2009**, *30*, 1-12.

424   [10]   J. Rutter, M. Reick, L. C. Wu, S. L. McKnight, *Science* **2001**, *293*, 510-514.

425   [11]   K. Nishio, T. Pornpitra, S. Izawa, T. Nishiwaki-Ohkawa, S. Kato, K. Hashimoto,

426   S. Nakanishi, *Plant Cell Physiol.* **2015**, *56*, 1053-1058.

427   [12]   a) T. Ooga, H. Sato, A. Nagashima, K. Sasaki, M. Tomita, T. Soga, Y. Ohashi,

428   *Mol Biosyst* **2011**, *7*, 1217-1223; b) Y. Ohashi, A. Hirayama, T. Ishikawa, S.

429   Nakamura, K. Shimizu, Y. Ueno, M. Tomita, T. Soga, *Mol Biosyst* **2008**, *4*,

430   135-147.

431   [13]   M. Sugimoto, D. T. Wong, A. Hirayama, T. Soga, M. Tomita, *Metabolomics*

432   **2010**, *6*, 78-95.

433   [14]   B. H. Junker, C. Klukas, F. Schreiber, *BMC Bioinformatics* **2006**, *7*, 109.

434

435

436